Journal of Materials Chemistry

Cite this: J. Mater. Chem., 2012, 22, 22258

www.rsc.org/materials

PAPER

Charge transport in amorphous and smectic mesophases of dicyanovinyl-substituted oligothiophenes†

Manuel Schrader,[a] Christian Körner,[b] Chris Elschner[b] and Denis Andrienko*[a]

Received 22nd July 2012, Accepted 5th September 2012
DOI: 10.1039/c2jm34837c

By analyzing electrostatic and polarization effects in amorphous dicyanovinyl-substituted oligothiophenes, we conclude that local molecular dipole moments result in a large, spatially correlated, energetic disorder. This disorder increases with the number of thiophene units in the oligomer and leads to an unexpected reduction of charge carrier mobility in a more ordered (smectic) mesophase, observed for the longest of the studied oligomers (hexamers). This reduction in mobilities contradicts the common belief that more ordered phases of organic semiconductors have a better charge carrier mobility. In this particular case, the amorphousness leads to a better-connected charge percolating network, helping to bypass deep energetic traps. By comparing mobilities of amorphous and crystalline mesophases we conclude that vacuum deposited thin organic films have well ordered polycrystalline morphologies.

I. Introduction

Organic solar cells based on small molecules[1–5] have recently shown a substantial improvement of up to 10% efficiencies in tandem cells.[6,7] A particularly successful class of materials in this respect is that of dicyanovinyl-substituted oligothiophenes (DCV*n*Ts, see Fig. 1), where electron-withdrawing terminal groups are used to decrease the optical band gap. DCV*n*Ts have been synthesized with one to six thiophene units (n = 1–6) per molecule[8,9] and functionalized with various ligands in order to increase solubility and modify stacking behavior.

Since overall solar cell performance depends on the efficiency of hole and electron transport in the donor and acceptor, respectively,[10] it is important to understand what factors affect charge transfer and transport in this class of compounds.[11–15] In crystalline phases of DCV3T and DCV4T (and their methylated derivatives), hole mobility was shown to be very sensitive to the connectivity graph (defined by electronic coupling elements) and energetic disorder (determined by variations in site energies), which is due to large dipole moments of the terminal groups.[8,16,17] In solar cells, however, DCV*n*Ts and fullerenes are mixed in a thin film. The donor phase can either have a different morphology than in a single crystal molecular packing[18] or can be only partially ordered.[19]

Herein, we complement the studies of charge transport in crystalline materials by analyzing hole transport in *amorphous* mesophases of DCV*n*Ts, *i.e.*, systems with a completely disordered molecular alignment. We find that a large energetic disorder leads to low charge carrier mobilities, which decrease with the increase in the oligomer length. In sexithiophenes, $n = 6$, we observe a more ordered, smectic, mesophase in which molecules are aligned in planes. This mesophase not only has a lower energetic disorder than the amorphous mesophase but also a (substantially) lower mobility. Microscopic origins of this inconsistency are explained by comparing charge percolating networks of electronic coupling elements and spatially correlated energetic disorders of the two DCV6T mesophases.

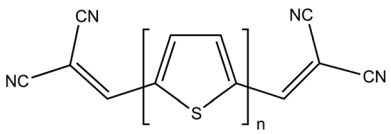

Fig. 1 Molecular structures of terminally dicyanovinyl-substituted oligothiophenes (DCV*n*T, n = 1–6).

II. Methodology

Atomistic molecular dynamic simulations are performed using the GROMACS simulation package[20] in the NPT ensemble with the Berendsen barostat,[21] stochastic velocity-rescaling thermostat,[22] and a re-parametrized version of the OPLS force field.[17] Amorphous systems of 4096 DCV*n*T molecules (n = 1–6) are first equilibrated at 800 K for 10 ns, well above their glass transition temperatures, quenched to 300 K, and then equilibrated for another 10 ns.

[a]*Max Planck Institute for Polymer Research, Ackermannweg 10, 55128 Mainz, Germany. E-mail: denis.andrienko@mpip-mainz.mpg.de*
[b]*Institut für Angewandte Photophysik, Technische Universität Dresden, George-Bähr-Str. 1, 01069 Dresden, Germany*
† Electronic supplementary information (ESI) available. See DOI: 10.1039/c2jm34837c

The longest of the compounds, DCV6T, is isotropic at 800 K, but spontaneously forms a smectic mesophase at 700 K. To avoid having defects in the smectic layers, we have pre-arranged molecules on a lattice and equilibrated the system at 700 K for 10 ns. The resulting molecular arrangement had the same spacing between the smectic layers as the one obtained by cooling it from the amorphous phase.

Molecular ordering is characterized by the order parameter, S, which is the largest eigenvalue of the order tensor, $S_{\alpha\beta} = \frac{1}{2}\langle 3n_\alpha n_\beta - \delta_{\alpha\beta}\rangle$. Note that the unit vector $\vec{n}$ is defined to be along the backbone of the molecule by the two branching carbons of the DCV groups. Order parameter values, summarized in Table 1, show that all amorphous morphologies are isotropic with $S < 0.1$, while the smectic phase of DCV6T has a preferred molecular orientation along the x-axis with $S = 0.81$. Two representative slices of the amorphous and smectic DCV6T morphologies are shown in Fig. 2a.

Charge carrier dynamics is modeled by evaluating intermolecular charge carrier hopping rates and solving the master equation for a charge carrier drift-diffusing in an applied electric field using the kinetic Monte Carlo algorithm.[23–28] The high-temperature limit of the Marcus theory[29,30] is employed to evaluate the transfer rates for the charge hopping between neighboring molecules (i and j),

$$\omega_{ij} = \frac{J_{ij}^2}{\hbar}\sqrt{\frac{\pi}{\lambda k_B T}}\exp\left[-\frac{(\Delta E_{ij} - \lambda)^2}{4\lambda k_B T}\right], \quad (1)$$

where $T = 300$ K, λ is the reorganization energy (given in Table 1 for all compounds), J_{ij} is the electronic coupling element, or transfer integral, and ΔE_{ij} is the site energy difference which has contributions from an external electric field and electrostatic interactions, including polarization. These microscopic quantities are calculated explicitly for each pair of molecules from the neighbor list using quantum-mechanical and polarizable force-field methods.[27] A pair of molecules is added to the list of neighbors if the distance between centers of mass of any of their thiophene or dicyanovinyl groups is below a cutoff of 0.8 nm. In particular, the electronic coupling elements, J_{ij}, are calculated using the semi-empirical ZINDO method.[31] Electrostatic contributions to the site energies are evaluated self-consistently based on the Thole model,[32] using the atomic polarizabilities and partial charges listed in the ESI.†

III. Results

A. Electronic coupling elements

We first analyze the electronic coupling elements, J_{ij}, between neighboring molecules. In the absence of energetic disorder, a graph with vertex positions given by the molecular centers of mass and edges weighted by the hopping rates (which are proportional to J_{ij}^2) should provide a complete description of the system needed to determine the charge carrier mobility.

Representative slices of a weighted graph are shown in Fig. 2b. Here the graph vertices are the molecular centers of mass and the color/thickness of the edges reflects the magnitude of the corresponding electronic coupling elements. One can see that the amorphous mesophase has a spatially uniform distribution of vertices, while the smectic phase comprises a set of well-interconnected two-dimensional planes (parallel to the yz-plane), connected with each other by a few edges more or less parallel to the x-axis. Note that the smectic phase has approximately two orders of magnitude higher electronic coupling elements within the layers than between them (corresponding distributions together with tabulated values can be found in the ESI†). The insets in Fig. 2b depict a set of sites accessible for a charge: a spherical shell (yellow) for the isotropic DCV6T, and a ring (red) in the same layer with two islands (blue) in the neighboring layers for the smectic mesophase of DCV6T.

B. Site energies

The acceptor–donor–acceptor molecular architecture of DCVnTs results in large dipole moments at the terminal groups. In combination with the disorder in molecular orientations this leads to a large, spatially correlated, energetic disorder.[17,33] Such an energetic landscape is shown in Fig. 2c for the amorphous and smectic phases of DCV6T. One can see that site energies are spatially correlated due to the long range nature of Coulomb forces.[34,35] For all systems, the distributions of site energy differences for pairs in the neighbor list have a Gaussian shape (shown in the ESI†). The widths of these distributions, σ, are summarized in Table 1 and shown in the right panel of Fig. 3a. It can be seen that this energetic disorder, σ, slightly increases with the number of thiophene units in the molecule and, as expected, the more ordered smectic phase of DCV6T has a lower energetic disorder than the amorphous DCV6T.

C. Charge mobility without energetic disorder

To understand the effect of the morphology and charge transfer parameters on charge carrier mobility, we first simulate charge dynamics in a system without energetic disorder and external field.

The largest and the smallest eigenvalues of the mobility tensor (which define the range of the variation of the mobility) are shown in the right panel of Fig. 3b. For amorphous systems, they lie in the range of 0.4–0.2 $cm^2\ V^{-1}\ s^{-1}$, hence they do not depend on the molecular length. When analyzing electronic couplings in

Table 1 Density, nematic order parameter, reorganization energy, energetic disorder, effective energetic disorder, and mobility

	DCV1T	DCV2T	DCV3T	DCV4T	DCV5T	DCV6T	DCV6T smectic
ρ, g cm^{-3}	1.17	1.22	1.25	1.27	1.29	1.30	1.33
S	0.02	0.02	0.02	0.02	0.06	0.04	0.81
λ, eV	0.17	0.17	0.18	0.21	0.22	0.23	0.23
σ, eV	0.25	0.28	0.29	0.30	0.33	0.35	0.33
σ_{eff}, eV	0.144	0.150	0.154	0.163	0.170	0.176	0.205
μ, $cm^2\ V^{-1}\ s^{-1}$	1.1×10^{-8}	1.1×10^{-9}	6.8×10^{-10}	3.5×10^{-10}	8.5×10^{-11}	1.3×10^{-11}	1.8×10^{-14}

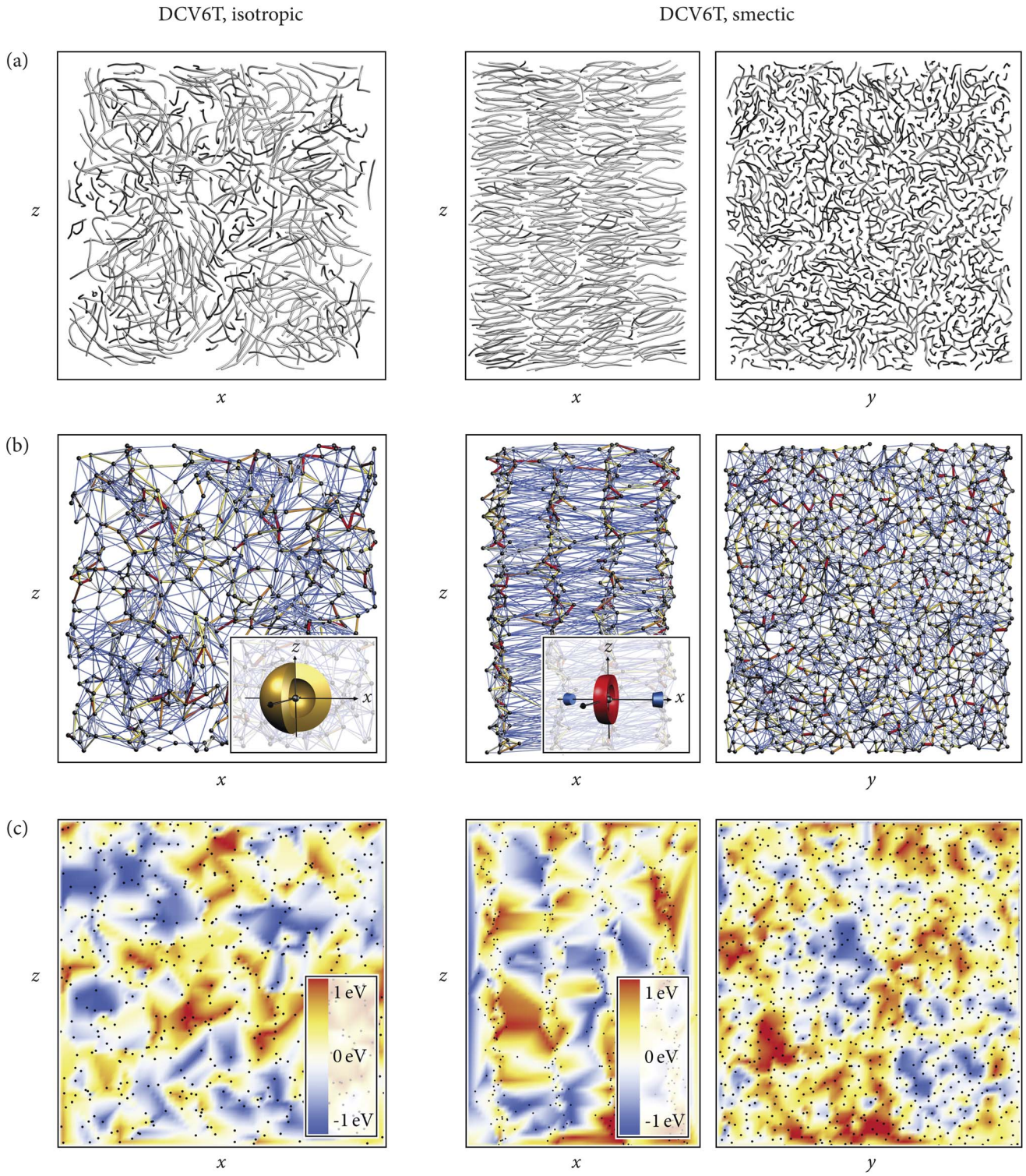

Fig. 2 (a) Equilibrated simulation boxes of the isotropic and smectic mesophases of DCV6T, where 2 nm thick slices of the system oriented perpendicular to the *y*-direction (and the *x*-direction for the smectic mesophase) are shown. (b) Hopping sites (molecular centers of mass) are depicted by dots and electronic coupling elements by edges. The insets illustrate the direction-resolved distributions of the nearest hopping sites. (c) Hopping sites and respective site energies (including polarization) depicted *via* the color map.

amorphous systems, we have concluded that the average separation between molecular centers of mass increases, while the average electronic coupling decreases with increasing n. For amorphous systems, these two effects apparently balance each other in the expression for the mobility tensor, $\mu_{\alpha\ \beta} = (k_B T)^{-1} \sum_{ij} p_i \omega_{ji} (r_{i,\alpha} r_{i,\beta} - r_{j,\alpha} r_{j,\beta})$, where p_i is the occupation probability of site i, and ω_{ij} is the charge transfer rate from site i to site j (according to eqn (1)).

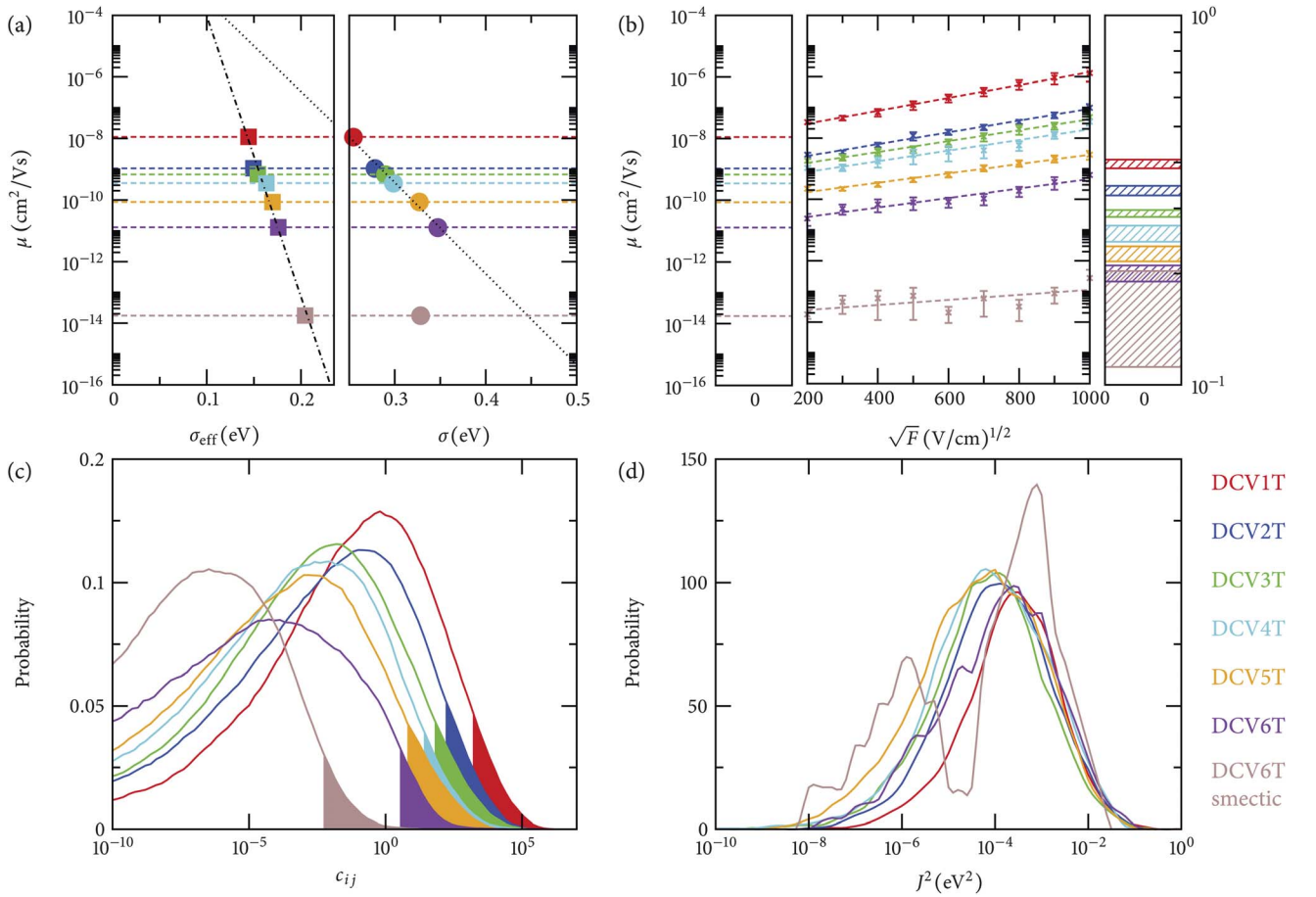

Fig. 3 (a) Semi-logarithmic plot of mobility *versus* an effective (left, introduced in Section IIIE) and neighbor-list based (right, defined in Section IIIB) energetic disorder. (b) Right: largest and smallest eigenvalues of the zero-field mobility tensor without the energetic disorder. Middle: Poole–Frenkel plots and linear fits used to extract the zero field mobility. Left: zero-field mobility in systems with energetic disorder. (c) Distribution of absolute values of edge currents, $|c_{ij}|$, where the edges contributing to 90% of the total edge current are shown by the filled areas. (d) Distributions of electronic couplings for those edges which contribute the most to the total current (filled areas in (c)).

The right panel of Fig. 3b also shows that the DCV6T smectic phase has a (uniaxial) mobility tensor with the largest eigenvalue of 0.21 $cm^2\ V^{-1}\ s^{-1}$ (along the *x*-axis) and 0.11 $cm^2\ V^{-1}\ s^{-1}$ in the *yz*-plane. Unexpectedly, the mobility along the *x*-axis is slightly higher than the mobility in the *yz*-plane, even though electronic couplings between the smectic planes are significantly lower. Again, larger hopping distances between the smectic layers compensate for the reduction in electronic couplings.

Another interesting observation is that the smectic ordering does not lead to a substantial increase of electronic coupling elements in smectic layers since molecular orientations in the *yz*-plane are also disordered (liquid-like) within these layers. However, smectic ordering results in smaller intermolecular separations within layers, and hence (small) mobility reduction as compared to the isotropic phase. This conclusion can be generalized by stating that, for efficient transport, *local* molecular ordering (*e.g.* crystallization in a smectic layer) is just as important as long-range ordering, *e.g.* such as the formation of the smectic mesophase.

D. Effect of energetic disorder

We now include the energetic disorder and study the field-dependence of mobility. The middle panel of Fig. 3b shows the Poole–Frenkel (log μ *vs.* $\sqrt{F}$) plots of hole mobility for all systems, and the left panel shows the extrapolated zero-field mobilities. As expected, in amorphous systems, energetic disorder leads to a mobility reduction by several orders of magnitude with a systematic mobility decrease as the energetic disorder σ increases. This is in agreement with the Gaussian disorder model (GDM), where rougher energetic landscapes lead to smaller charge carrier mobilities. Note, that in our case site energies are explicitly calculated and not chosen randomly from a Gaussian distribution.

The situation is, however, very different in the smectic phase. Here, the reduction in mobility is very large, resulting in values of 10^{-14} $cm^2\ V^{-1}\ s^{-1}$, despite the fact that the energetic disorder is *smaller* than in the amorphous DCV6T phase. This contradicts both the results of the GDM model and the common belief that more ordered phases of organic semiconductors should have a higher charge carrier mobility. In order to understand this behavior, we now analyze distributions of local currents in amorphous and smectic mesophases.

E. Spatial correlations and filamentary currents

To analyze edge currents, defined as $c_{ij} = \frac{1}{2}e(p_j\omega_{ji} - p_i\omega_{ij})$, we first sort all $|c_{ij}|$ values and then remove molecular pairs with

small currents until the remaining sum of the original total current reaches 0.9. By doing this, only the high-current edges which contribute to the 90% of the total current in the system are left. Fig. 3c shows that only a small fraction of all edges (neighbor list pairs) is actually used by a drift-diffusing charge (filled area). These edge currents are visualized in Fig. 4a for an amorphous morphology of DCV4T.

Such a reduction in the number of pairs participating in charge transport can be attributed to the long-range nature of electrostatic interactions: site energies become spatially correlated and charges move in the areas of low site energies. This can be seen in Fig. 4b, where the current filament is shown together with the cross-section of the site energy landscape. The filament clearly avoids the energetically unfavorable regions and percolates along the edges with large electronic couplings.

For the remaining edges, *i.e.*, the high-current edges contributing to 90% of the current, the distributions of site energy differences were again evaluated. The widths of these distributions, σ_{eff}, are summarized in Table 1 and are also shown in Fig. 3a (left panel). This effective energetic disorder is significantly lower than the disorder evaluated for all neighboring pairs (right panel). Hence, we can conclude that, even for an amorphous morphology, characterization of the system by the site energy distribution alone can be misleading.

By comparing the two different phases of DCV6T, one can see that the effective energetic disorder for the smectic phase is now higher than that of the isotropic phase. In fact, it is now possible to correlate $\log(\mu)$ with the effective value of the disorder, as shown in the left panel of Fig. 3a. If spatial correlations and the topology of the charge percolating

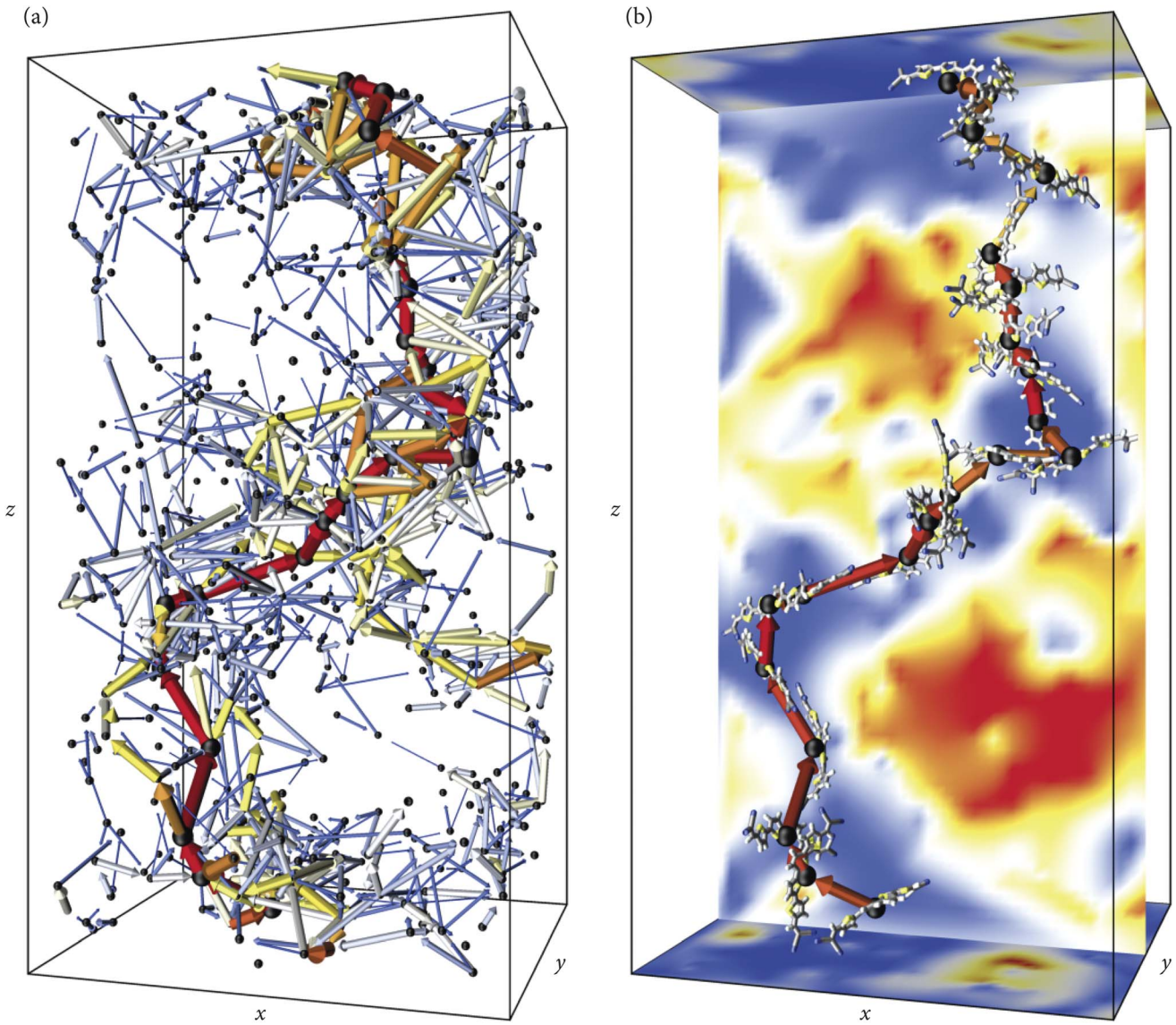

Fig. 4 (a) Local currents contributing to 90% of the total current in an amorphous DCV4T system. An electric field of 1000 $(\text{V/cm})^2$ is applied in the z-direction. The dots are the molecular centers of mass, arrows depict local currents (their thickness and color are proportional to the logarithm of the current amplitude). (b) Current filament and energetic landscape in a slice of the system. The charge carrier traverses the system in the z-direction (13.7 nm) by hopping along the 21 molecules shown.

network are not taken into account, this would clearly not be possible (see Fig. 3a, right panel).

One can also analyze the distributions of effective transfer integrals, $\langle J_{ij}^2 \rangle_{\text{eff}}$, which are shown in Fig. 3d. These are very similar for all amorphous systems. For a smectic DCV6T, the distribution is bimodal. The peak with higher values corresponds to the edges in the smectic layer (*yz*-plane) and the peak with smaller values corresponds to the edges along the *x*-direction, perpendicular to these layers. The correlated energetic disorder and the bimodal distribution of transfer integrals are therefore the microscopic reasons for the mobility reduction in the smectic phase. The energetic landscape in both amorphous and smectic phases is spatially correlated in all three dimensions, *i.e.* current filaments can be thought of as three-dimensional random walks. This also agrees with the observation that the mobility tensor of the smectic system is practically isotropic. In the smectic phase, however, transfer integrals between the layers are significantly smaller than within the layers. Thus, the carrier is biased to drift-diffuse within the layers, that is two-dimensional cross-sections of the energetic landscape. Hence, the energetic disorder in the smectic phase is effectively higher and therefore the transport becomes slower.

IV. Discussion and conclusions

In summary, we have characterized networks of electronic couplings and energetic landscapes for a series of amorphous dicyanovinyl-substituted oligothiophenes and a smectic mesophase of a compound with six thiophenes.

All amorphous phases have a large, spatially correlated, energetic disorder, resulting in a filamentary structure of microscopic currents. The value of the disorder and reorganization energy increases with the number of thiophene units in the molecule, leading to smaller values of charge carrier mobility for longer molecules.

A more ordered smectic phase of DCV6T has a lower energetic disorder but (unexpectedly) significantly lower charge mobility than that of the amorphous DCV6T. This can be explained as an interplay between the three-dimensional spatial correlations of the energetic disorder and the two-dimensional network of coupling elements within smectic layers which have small electronic couplings between them.

In fact, a similar observation has already been made for crystalline compounds.[17] There, strong one-dimensional couplings along the π-stacking direction have shown to lead to a lower mobility as compared to methylated compounds without pronounced π-stacking, but with a more balanced (three-dimensional) network of suitable electronic couplings. Here, stronger electronic couplings in smectic layers (two-dimensional percolating network) suppress electronic couplings between the layers, which, in combination with a large energetic disorder, leads to an overall reduction of the charge carrier mobility.

We finally compare the energetic disorder and mobilities of amorphous and crystalline DCV3T and DCV4T. In crystalline compounds,[17] DCV3T and DCV4T have energetic disorders of 0.11 eV and 0.10 eV, respectively. These are significantly smaller than their energetic disorders in the respective amorphous phases, 0.29 eV and 0.30 eV. As a result, the corresponding mobilities of the crystalline phases ($\sim 10^{-3}$ cm^2 V^{-1} s^{-1}) are more than six orders of magnitude higher. Though a qualitative conclusion is anticipated, the quantitative increase of mobility due to crystalline ordering and decrease of the energetic disorder is striking. Interestingly, the experimentally measured OFET mobility is of the order of $\sim 10^{-4}$ cm^2 V^{-1} s^{-1} for DCV4T,[16] indicating that thin organic films used in devices have well ordered polycrystalline morphologies, which is in agreement with recent X-ray scattering experiments.[36]

Acknowledgements

This work was partially supported by the DFG program IRTG 1404, DFG grant SPP 1355, and BMBF grant MESOMERIE. We are grateful to Mara Jochum, Björn Baumeier, Pascal Kordt, Anton Melnyk, and Carl Pölking for critical reading of the manuscript.

References

1 H. Bürckstümmer, N. M. Kronenberg, M. Gsänger, M. Stolte, K. Meerholz and F. Würthner, *J. Mater. Chem.*, 2010, **20**, 240.
2 V. Steinmann, N. M. Kronenberg, M. R. Lenze, S. M. Graf, D. Hertel, H. Bürckstümmer, F. Würthner and K. Meerholz, *Appl. Phys. Lett.*, 2011, **99**, 193306.
3 V. Steinmann, N. M. Kronenberg, M. R. Lenze, S. M. Graf, D. Hertel, K. Meerholz, H. Bürckstümmer, E. V. Tulyakova and F. Würthner, *Adv. Eng. Mater.*, 2011, **1**, 888–893.
4 A. Mishra and P. Bäuerle, *Angew. Chem., Int. Ed.*, 2012, **51**, 2020.
5 Y. Sun, G. C. Welch, W. L. Leong, C. J. Takacs, G. C. Bazan and A. J. Heeger, *Nat. Mater.*, 2012, **11**, 44.
6 R. F. Service, *Science*, 2011, **332**, 293.
7 Heliatek GmbH press release, http://www.heliatek.com, 2011.
8 R. Fitzner, E. Reinold, A. Mishra, E. Mena-Osteritz, H. Ziehlke, C. Körner, K. Leo, M. Riede, M. Weil and O. Tsaryova, *et al.*, *Adv. Funct. Mater.*, 2011, **21**, 897.
9 M. M. Bader, P.-T. T. Pham and E. H. Elandaloussi, *Cryst. Growth Des.*, 2010, **10**, 5027.
10 J.-L. Brédas, J. E. Norton, J. Cornil and V. Coropceanu, *Acc. Chem. Res.*, 2009, **42**, 1691.
11 J.-L. Brédas, D. Beljonne, V. Coropceanu and J. Cornil, *Chem. Rev.*, 2004, **104**, 4971.
12 D. Beljonne, J. Cornil, L. Muccioli, C. Zannoni, J.-L. Brédas and F. Castet, *Chem. Mater.*, 2010, **23**, 591.
13 M. Lamarra, L. Muccioli, S. Orlandi and C. Zannoni, *Phys. Chem. Chem. Phys.*, 2012, **14**, 5368.
14 B. Baumeier, D. Andrienko and M. Rohlfing, *J. Chem. Theory Comput.*, 2012, **8**, 2790.
15 B. Baumeier, D. Andrienko, Y. Ma and M. Rohlfing, *J. Chem. Theory Comput.*, 2012, **8**, 997.
16 R. Fitzner, C. Elschner, M. Weil, C. Uhrich, C. Körner, M. Riede, K. Leo, M. Pfeiffer, E. Reinold and E. Mena-Osteritz, *et al.*, *Adv. Mater.*, 2012, **24**, 675–680.
17 M. Schrader, R. Fitzner, M. Hein, C. Elschner, B. Baumeier, K. Leo, M. Riede, P. Bäuerle and D. Andrienko, *J. Am. Chem. Soc.*, 2012, **134**, 6052.
18 C. Elschner, M. Schrader, R. Fitzner, M. Hein, A. A. Levin, P. Bäuerle, D. Andrienko, K. Leo and M. Riede, 2012, submitted.
19 H. Ziehlke, R. Fitzner, C. Körner, R. Gresser, E. Reinold, P. Bäuerle, K. Leo and M. K. Riede, *J. Phys. Chem. A*, 2011, **115**, 8437.
20 B. Hess, C. Kutzner, D. van der Spoel and E. Lindahl, *J. Chem. Theory Comput.*, 2008, **4**, 435.
21 H. J. C. Berendsen, J. P. M. Postma, W. F. van Gunsteren, A. DiNola and J. R. Haak, *J. Chem. Phys.*, 1984, **81**, 3684.
22 G. Bussi, D. Donadio and M. Parrinello, *J. Chem. Phys.*, 2007, **126**, 014101.

23 J. Kirkpatrick, V. Marcon, J. Nelson, K. Kremer and D. Andrienko, *Phys. Rev. Lett.*, 2007, **98**, 227402.
24 T. Vehoff, Y. S. Chung, K. Johnston, A. Troisi, D. Y. Yoon and D. Andrienko, *J. Phys. Chem. C*, 2010, **114**, 10592.
25 T. Vehoff, B. Baumeier, A. Troisi and D. Andrienko, *J. Am. Chem. Soc.*, 2010, **132**, 11702.
26 A. Lukyanov and D. Andrienko, *Phys. Rev. B: Condens. Matter Mater. Phys.*, 2010, **82**, 193202.
27 V. Rühle, A. Lukyanov, F. May, M. Schrader, T. Vehoff, J. Kirkpatrick, B. Baumeier and D. Andrienko, *J. Chem. Theory Comput.*, 2011, **7**, 3335.
28 B. Baumeier, F. May, C. Lennartz and D. Andrienko, *J. Mater. Chem.*, 2012, **22**, 10971.
29 R. A. Marcus, *Rev. Mod. Phys.*, 1993, **65**, 599.
30 G. R. Hutchison, M. A. Ratner and T. J. Marks, *J. Am. Chem. Soc.*, 2005, **127**, 2339.
31 J. Kirkpatrick, *Int. J. Quantum Chem.*, 2007, **108**, 51.
32 B. Thole, *Chem. Phys.*, 1981, **59**, 341.
33 Y. Nagata and C. Lennartz, *J. Chem. Phys.*, 2008, **129**, 034709.
34 S. V. Novikov, D. H. Dunlap, V. M. Kenkre, P. E. Parris and A. V. Vannikov, *Phys. Rev. Lett.*, 1998, **81**, 4472.
35 S. V. Novikov and A. V. Vannikov, *J. Phys. Chem.*, 1995, **99**, 14573.
36 C. Koerner, C. Elschner, N. C. Miller, R. Fitzner, F. Selzer, E. Reinold, P. Bäuerle, M. F. Toney, M. D. McGehee and K. Leo, *et al.*, *Org. Electron.*, 2012, **13**, 623.

